Experiments for the Reduction of Wind Tunnel Wall Interference by Adaptive-Wall Technology

E. M. Kraft and R. L. Parker, Jr.
ARO, Inc.

October 1979

Final Report for Period October 1977 — September 1978

**ARNOLD ENGINEERING DEVELOPMENT CENTER
ARNOLD AIR FORCE STATION, TENNESSEE
AIR FORCE SYSTEMS COMMAND
UNITED STATES AIR FORCE**

This report has been reviewed by the Information Office (OI) and is releasable to the National Technical Information Service (NTIS). At NTIS, it will be available to the general public, including foreign nations.

APPROVAL STATEMENT

This report has been reviewed and approved.

ALEXANDER F. MONEY
Project Manager
Directorate of Technology

Approved for publication:

FOR THE COMMANDER

MARION L. LASTER
Director of Technology
Deputy for Operations

REPORT DOCUMENTATION PAGE

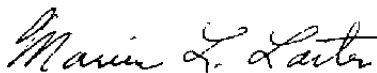| 1. REPORT NUMBER	2. GOVT ACCESSION NO.	3. RECIPIENT'S CATALOG NUMBER
AEDC-TR-79-51		

4. TITLE (and Subtitle)	5. TYPE OF REPORT & PERIOD COVERED
EXPERIMENTS FOR THE REDUCTION OF WIND TUNNEL WALL INTERFERENCE BY ADAPTIVE WALL TECHNOLOGY	Final Report – October 1977 – September 1978
	6. PERFORMING ORG. REPORT NUMBER

7. AUTHOR(s)	8. CONTRACT OR GRANT NUMBER(s)
E. M. Kraft and R. L. Parker, Jr., ARO, Inc., a Sverdrup Corporation Company	

9. PERFORMING ORGANIZATION NAME AND ADDRESS	10. PROGRAM ELEMENT, PROJECT, TASK AREA & WORK UNIT NUMBERS
Arnold Engineering Development Center/DOT Air Force Systems Command Arnold Air Force Station, Tennessee 37389	Program Element 65807F

11. CONTROLLING OFFICE NAME AND ADDRESS	12. REPORT DATE
Arnold Engineering Development Center/DOS Air Force Systems Command Arnold Air Force Station, Tennessee 37389	October 1979
	13. NUMBER OF PAGES
	40

14. MONITORING AGENCY NAME & ADDRESS(if different from Controlling Office)	15. SECURITY CLASS. (of this report)
	UNCLASSIFIED
	15a. DECLASSIFICATION/DOWNGRADING SCHEDULE N/A

16. DISTRIBUTION STATEMENT (of this Report)

Approved for public release; distribution unlimited.

17. DISTRIBUTION STATEMENT (of the abstract entered in Block 20, if different from Report)

18. SUPPLEMENTARY NOTES

Available in DDC

19. KEY WORDS (Continue on reverse side if necessary and identify by block number)

wind tunnels	porosity
transonic flow	airfoils
walls	
configurations	

20 ABSTRACT (Continue on reverse side if necessary and identify by block number)

Experiments were conducted in the AEDC Aerodynamic Wind Tunnel (1T) to evaluate the applicability of adaptive-wall technology to reduce wall interference in a transonic wind tunnel. Data were obtained on a six-percent-blockage, two-dimensional, NACA 0012 airfoil section with two different, adaptable porous wall configurations. One configuration featured variable longitudinal control of the local hole angle and the other

DD FORM 1473 EDITION OF 1 NOV 65 IS OBSOLETE
1 JAN 73

20. ABSTRACT (Continued)

featured global porosity control. The experiments demonstrated
that adaptive-wall techniques could be used to significantly
reduce wall interference effects. Although neither wall
configuration could be adjusted to duplicate the pressure
distributions (calculated at the tunnel boundary control surface
with adaptive-wall technology) to produce interference-free
conditions, matching the pressure level upstream of the model and
minimum pressure in the vicinity of the model adequately reduced
the wall interference. One of the most effective means for
matching these global parameters was plenum pressure adjustment;
thus, some refinement may be obtained through segmented plena
control.

AFSC
Arnold AFS Tenn.

PREFACE

The work reported herein was conducted by the Arnold Engineering Development Center (AEDC), Air Force Systems Command (AFSC), for the Directorate of Technology (AEDC/DOT). The results were obtained by ARO, Inc., AEDC Division (a Sverdrup Corporation Company), operating contractor for the AEDC, AFSC, Arnold Air Force Station, Tennessee, under ARO Project Numbers P32A-J6A and P32A-S3A. The Air Force project manager was Mr. A. F. Money, AEDC/DOT. The manuscript was submitted for publication on May 22, 1979.

CONTENTS

ILLUSTRATIONS

Figure

1.0 INTRODUCTION

The demand for higher quality data on increasingly sophisticated aerodynamic configurations has made obvious the limitations of transonic test capability. Smaller design margins are placed on current aircraft that incorporate high-lift transonic wings and that operate at extreme attitudes during maneuvering conditions; this necessitates more accurate test data at those wind tunnel conditions most susceptible to interfering inputs. In recent years, the emphases in development of a large transport configuration have been on increasing efficiency with a cruise speed in the transonic range and on improving the quality of the transonic wind tunnel data.

Of particular concern is the effect of tunnel boundaries. Despite significant advances in methods for computing wall interference effects (Ref. 1), the primary reasons for not applying analytical corrections for interference effects in transonic testing are

1. The validity of the classical linear homogeneous boundary condition for a ventilated wall commonly used in the analyses is questionable, especially for highly distorted flow fields around high lift models.

2. The value of the characteristic porosity parameter used in the analytical methods is typically unknown for a perforated wall wind tunnel. In addition, there is the important question of whether there exists for a given flow field in the wind tunnel (particularly a shock-infested, separated flow), a corresponding free-air flow field determined by simple corrections to Mach number and angle of attack.

The general practice, consequently, has been to restrict the maximum value of the model blockage ratio to ≤ 1 percent. However, Binion and Lo (Ref. 2) and Binion (Ref. 3) have indicated that for even a 1-percent-blockage model there can be significant wall effects on the pressure distribution over the model for near-sonic Mach numbers.

There are, however, several important conclusions derivable from the analytical wall interference studies:

1. The optimum porosity for zero interference in a perforated-wall wind tunnel depends on the Mach number (Ref. 4). This was established experimentally by Jacocks (Refs. 5 and 6).

2. Generally, solid blockage, lift interference, and pitching-moment interference cannot be eliminated simultaneously with a single uniform porosity distribution. Lo (Ref. 7) and Lo and Glassman (Ref. 8) demonstrated, however, that lift and pitching-moment interference can be eliminated simultaneously by a proper longitudinal distribution of porosity.

3. The porosity parameter required for zero-blockage interference at transonic speeds was dependent on the model configuration. For example, it was shown theoretically (Ref. 9) that at a Mach number of 0.83 the porosity parameter required for zero-blockage interference on a biconvex airfoil could produce almost a 10-percent error in the shock location on an NACA 0012 airfoil. That two different models require two sets of optimum porosity schedules was demonstrated experimentally and reported in Refs. 5 and 6, respectively.

The ideal wall for zero-interference wind tunnel testing must be adjusted for different Mach numbers and model configurations and must possess a spatially variable wall characteristic.

Recently, Ferri and Baronti (Ref. 10) and Sears (Ref. 11) independently arrived at an adaptive-wall concept recognizing that local wall properties can be systematically adjusted to achieve unconfined flow through measuring two flow disturbance quantities and evaluating the requisite functional relationships for unconfined flow. Numerical simulation by Erickson and Nenni (Ref. 12) established the feasibility of the concept. Lo and Kraft (Ref. 13) showed the convergence of the concept to unconfined flow. Experimental studies (Refs. 14, 15, and 16) firmly validated the practicality of an adaptive-wall tunnel. The purpose of this report is to present results of some initial experiments using adaptive-wall technology to reduce wall interference.

2.0 ADAPTIVE-WALL CONCEPT

According to the adaptive-wall concept, to ascertain whether unconfined flight conditions are obtained in any wind tunnel, for any model configuration, it must be determined whether the measured flow variables at a convenient surface, S, away from the model and near the walls are consistent with flow in an unconfined region outside the tunnel. To make this determination, the distributions of two flow variables (such as the velocity components parallel and perpendicular to the surface S) are measured at S; one is used as the boundary value to specify uniquely the flow field exterior to S at unconfined, undisturbed flow of a uniform stream at infinity. Since the two measured distributions constitute redundant boundary data in the presence of the exterior region, far-field, boundary condition, equality at S of the measured flow variables interior to S and the

computed flow variables exterior to S constitutes a definition of interference-free flow in the wind tunnel. Therefore, by comparing the exterior region calculated values to the measured values of the same quantities, it can be determined whether unconfined-flow conditions exist in the tunnel.

Unconfined-flow conditions can be achieved if provisions are made for adjusting the wall boundary as necessary. A basic iterative scheme for applying the adaptive-wall technique to achieve unconfined flow is presented in Fig. 1. The axial and normal components, u and v, respectively, of the disturbance velocity are assumed to be the flow variables of interest at S. First a flow field is established in the tunnel, and the velocity components u_T and v_T are measured at the given control surface S. The exterior unconfined region is then evaluated by specifying $v_E = v_T$ as the boundary value at S. If the distribution at S of u_E determined from the exterior region calculation does not agree with u_T, then the flow is still constrained at the walls and the wall boundary must be readjusted. The iteration continues until u_E and u_T agree. Then the flow about the model in the tunnel is unconfined. The relaxation factor, k, is introduced to accelerate convergence of the iterative process as discussed in Ref. 13.
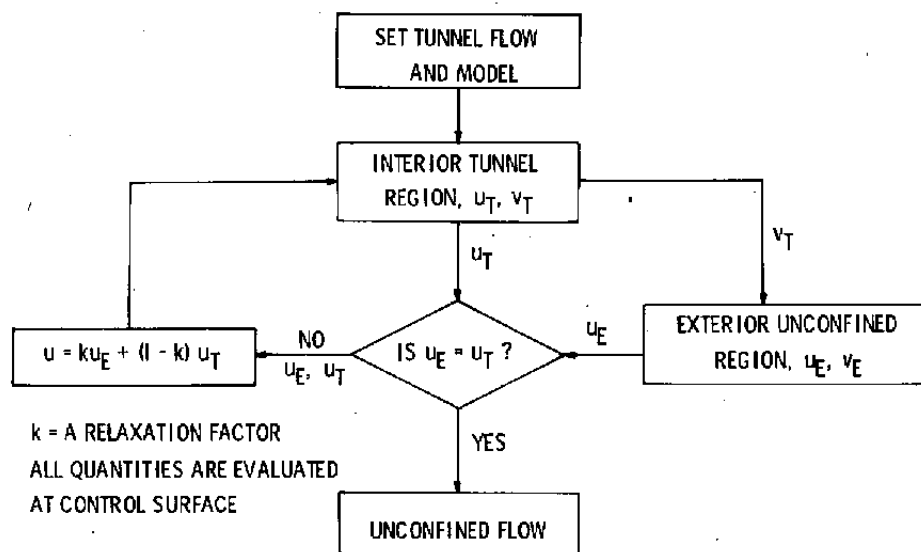
Figure 1. Basic iterative scheme for adaptive-wall concept.

Alternatively, $u_E = u_T$ could be specified at S in the exterior region and v_E compared with v_T to determine whether unconfined flow exists in the tunnel. More generally, any two conveniently measured flow variables can be used in the adaptive-wall process. The approach is valid for both two- and three-dimensional flow fields.

Application of the adaptive-wall concept requires the following in addition to the standard equipment for wind tunnel testing: (1) adaptive walls, (2) measurement devices for two flow variables at the reference surface, S, and (3) a computational method for evaluating the requisite functional relationships for the two flow variables in the unconfined external regions.

3.0 APPARATUS

3.1 AERODYNAMIC WIND TUNNEL (1T)

The experiments were conducted in the Aerodynamic Wind Tunnel (1T), which is a continuous-flow, nonreturn wind tunnel equipped with a two-dimensional, flexible nozzle and an auxiliary plenum evacuation system. The test section is of square cross section nominally 12 in. square and 37.5 in. long. The tunnel is operated at a total pressure of approximately 2,850 psfa. The stagnation temperature can be varied from 80 to 120°F above ambient temperature to prevent visible condensation from occurring in the test section. The tunnel arrangement is shown in Fig. 2.
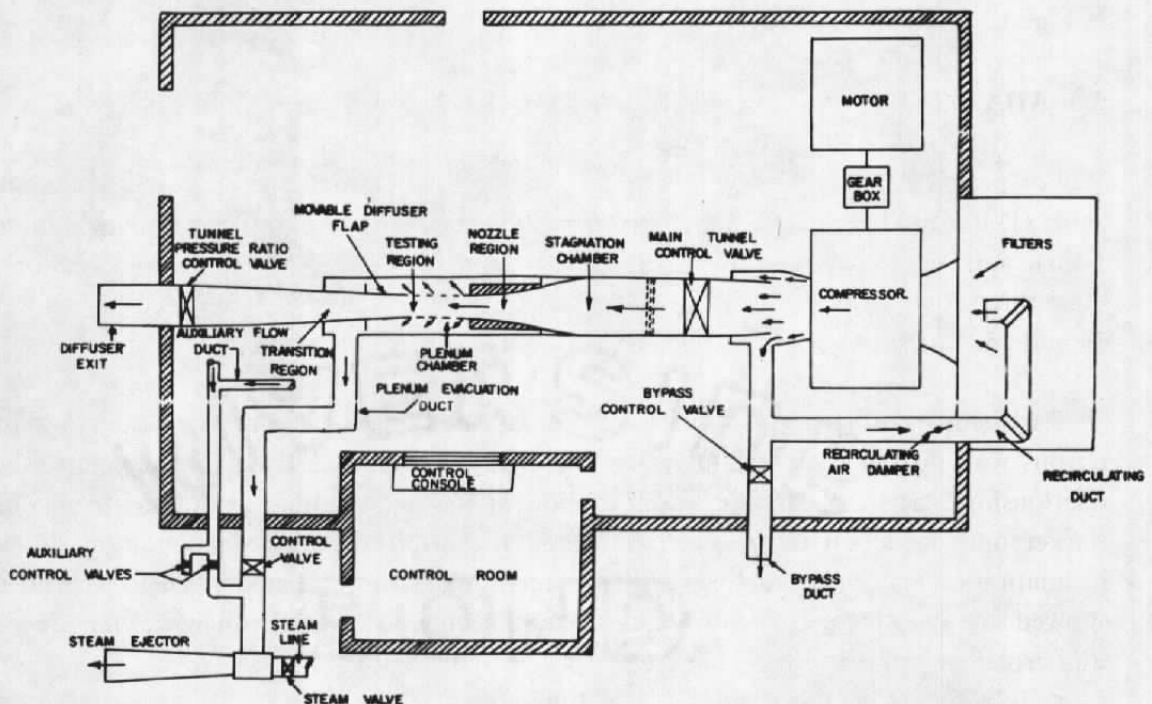
Figure 2. Aerodynamic Wind Tunnel (1T).

8

3.2 MODEL

For these initial experiments with the adaptive-wall concept, a two-dimensional model was selected for compliance with existing computational techniques and to minimize complexity of wall hardware and reference plane measuring devices. A 6-in.-chord NACA 0012 airfoil was chosen specifically since

1. The NACA 0012 profile has been shown to be relatively insensitive to Reynolds number effects above 2×10^6-chord Reynolds number (Ref. 17).

2. The profile shape and size are equivalent to the model used in the Calspan experiments (Ref. 14) and, hence, data from Ref. 18 could be used for comparison.

3. The profile shape and size (6-percent blockage) should produce significant wall interference effects at transonic speeds.

The geometric details and locations of the static pressure orifices on the model are illustrated in Fig. 3.

3.3 ADAPTIVE-WALL CONFIGURATIONS

For practical applications, three distinct methods for producing adaptive-wall control exist: (1) localized plenum pressure control, (2) localized wall contour control (streamlined walls), and (3) local crossflow characteristic control. In addition, some combination of these three could be used. Methods (1) and (2) have been investigated, respectively, in Refs. 14 and 15. In the present experiments, method (3) was investigated.

Early studies of perforated walls (Ref. 19) indicated that varying the open-area ratio of a porous wall does not significantly alter the crossflow characteristic (pressure-flow-angle relationship), whereas varying the inclination of the perforations to the airstream does. Parker and Jacocks (Ref. 20) demonstrated the effects of an axial variation of hole inclination on transonic flow over a three-dimensional, wing-tail model. Their experiments showed that the wing pressure distribution could be altered significantly by varying the local wall crossflow characteristics.

Based on these results, a longitudinally variable hole angle (LVHA) wall was developed at AEDC. The basic design of the LVHA wall is shown in Fig. 4. The LVHA wall consists of multiple rows of bored spheres connected by rods in the direction normal to the longitudinal

PROFILE GEOMETRY: $\pm y = 0.72\,(1.4845\,\sqrt{X} - 0.6300X - 1.7580X^2 + 1.4215\,X^3 - 0.5075X^4)$, in.

X/c	X, in.	± y, in.	X/c	X, in.	± y, in.
0.0000	0.0000	0.00000	0.4000	2.4000	0.3481
0.0125	0.0750	0.11364	0.5000	3.0000	0.3176
0.0250	0.1500	0.15690	0.6000	3.6000	0.2737
0.0500	0.3000	0.21330	0.7000	4.2000	0.2198
0.0750	0.4500	0.25200	0.8000	4.8000	0.1573
0.1000	0.6000	0.28098	0.9000	5.4000	0.0868
0.1500	0.9000	0.32070	0.9500	5.7000	0.0484
0.2000	1.2000	0.34422	1.0000	6.0000	0.0075
0.3000	1.8000	0.36012	L.E. Radius = 0.0948 in.		

NOMINAL ORIFICE SIZE 0.015 in.

PRESSURE ORIFICE LOCATIONS
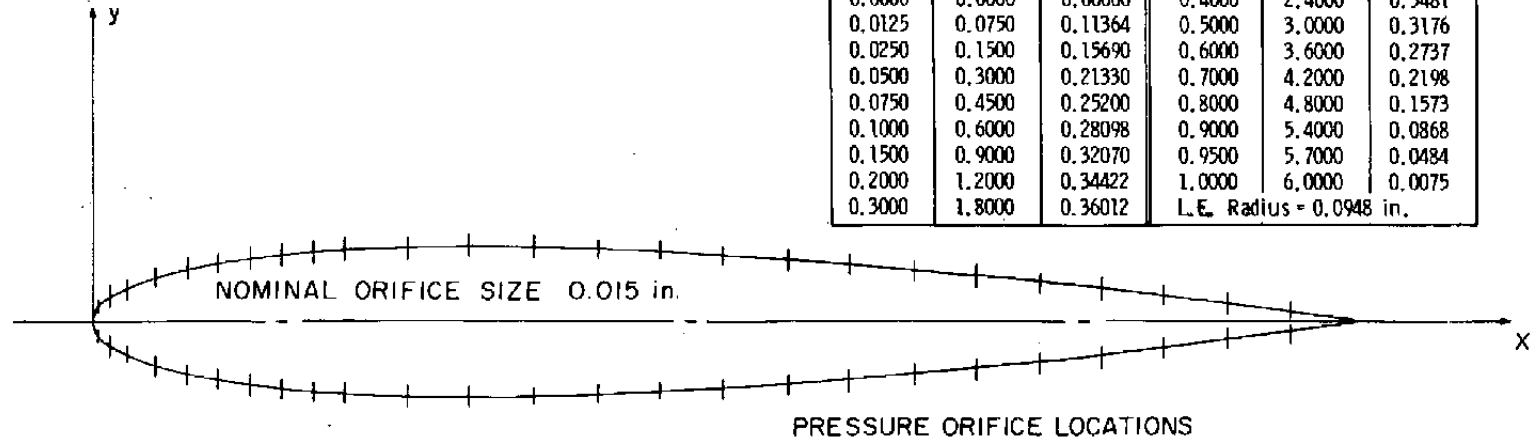
X/c	X, in.	X/c	X, in.
0.0000	0.0000	0.3500	2.100
0.0050	0.0277	0.4000	2.400
0.0125	0.0750	0.4500	2.700
0.0250	0.1500	0.5000	3.000
0.0500	0.3000	0.5500	3.300
0.0750	0.4500	0.6000	3.600
0.1000	0.6000	0.6500	3.900
0.1250	0.7500	0.7000	4.200
0.1500	0.9000	0.7500	4.500
0.1750	1.0500	0.8000	4.800
0.2000	1.2000	0.8500	5.100
0.2500	1.5000	0.9000	5.400
0.3000	1.8000	0.9500	5.700

Figure 3. Model geometry.

axis of the test section. The system of spheres is sandwiched between porous plates. By individual rotation of the rods, the hole angle and, hence, the crossflow characteristic can be locally controlled. The LVHA wall offered a means of active wall control for the preliminary adaptive-wall experiments.
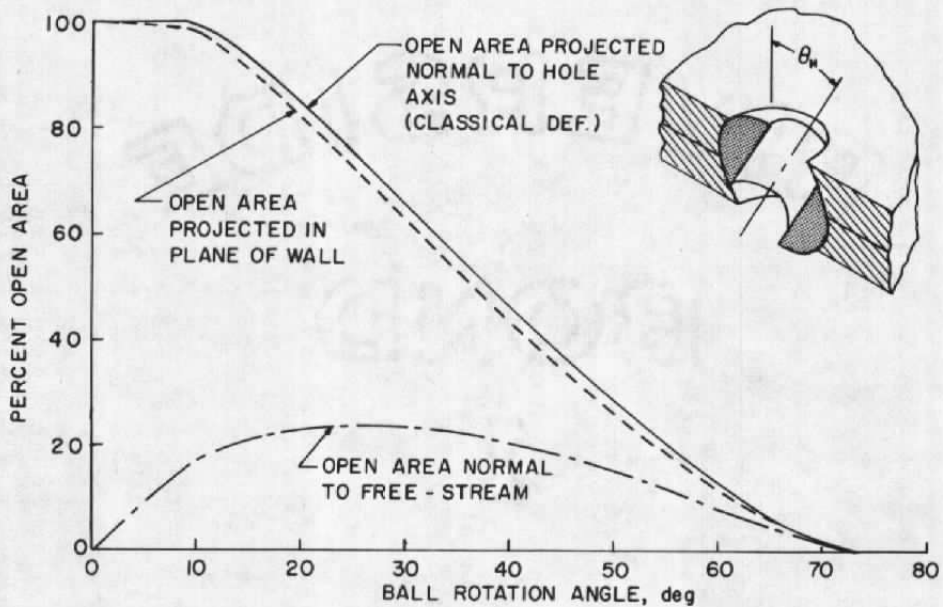
a. Variable porosity through rotary motion
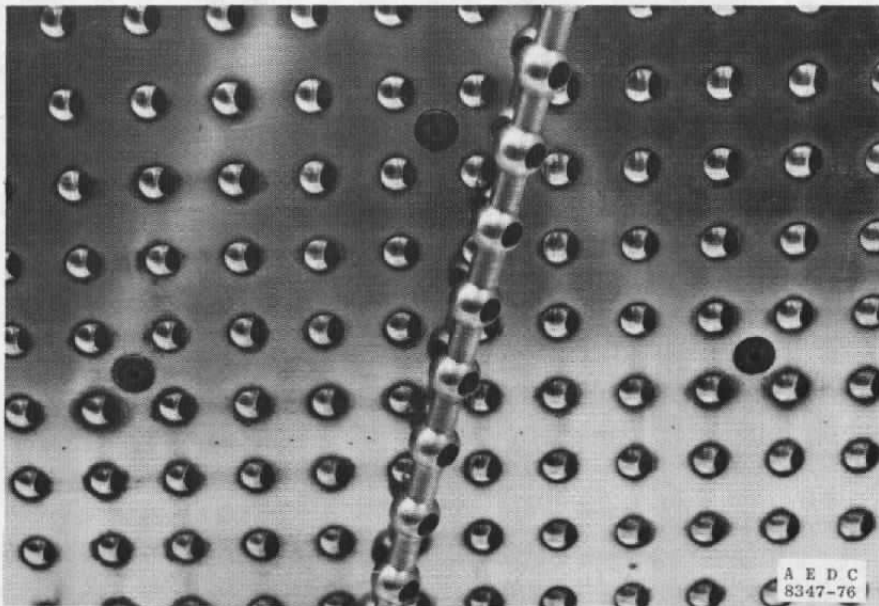
b. LVHA wall assembly

Figure 4. Longitudinally variable hole angle wall.

11

During the course of the adaptive-wall experiments, globally variable-porosity walls based on the walls used in the AEDC Aerodynamic Wind Tunnel (4T) were also employed. These walls — herein referred to as the variable-porosity walls — consist of two match-drilled plates with the airside plate held stationary and the backside, or cutoff plate, translated streamwise to achieve variations in porosity. Figure 5 shows two views illustrating these details.

The LVHA walls and the 4T walls were installed on the floor and ceiling of the test section. The sidewalls were solid.
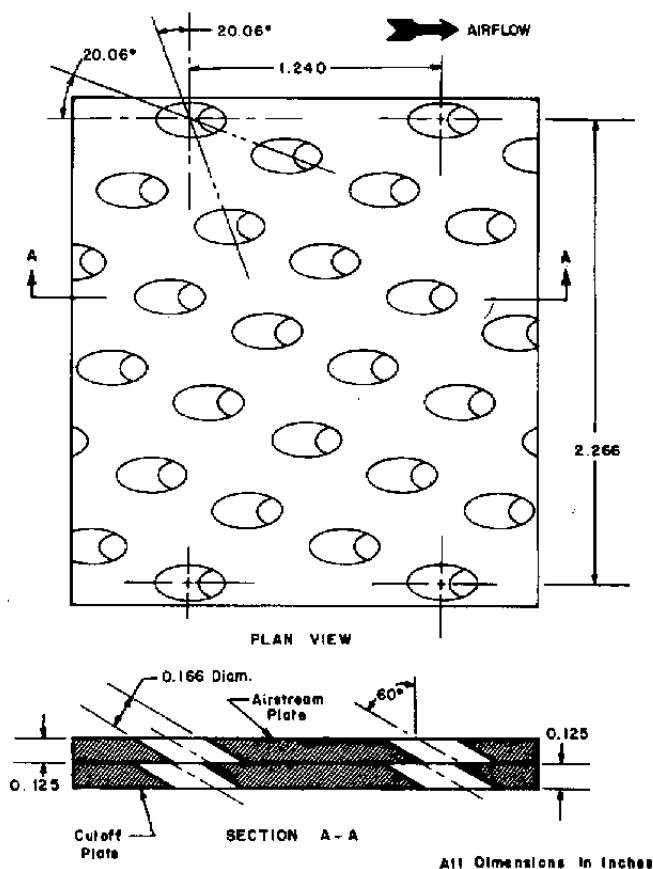
Figure 5. Variable-porosity wall.

3.4 CONTROL SURFACE FLOW VARIABLE SENSORS

Using the adaptive-wall concept requires the measurement of two flow variables at a reference surface, S, near the tunnel boundary. For a two-dimensional-model experiment, the surface, S, is conveniently defined by two surfaces ($y = \pm h$) parallel to the tunnel axis near the upper and lower walls. In the present experiments, the static pressure and flow angle at S were selected as the two independent flow variables.

The distribution of static pressure at the control surfaces was measured by two 0.5-in.-diam static pipes located parallel to the tunnel centerline. Each static pipe had 30 orifices oriented toward the plane of the wing. During the experiments, a brief study was made of the effect of rotating the orifices toward the tunnel wall; no appreciable effects were discerned. The pressure coefficient from the pressure measurement of the pipe is accurate to within ±0.01. Details of the static pipe installation and locations of the orifices are shown in Fig. 6.

ALL DIMENSIONS IN INCHES

ORIFICE LOCATION TUNNEL STATION		
0.00	18.05	23.56
4.83	18.60	24.11
7.58	19.15	24.66
9.78	19.70	25.77
11.99	20.26	26.86
13.07	20.81	27.97
14.19	21.36	29.07
15.30	21.91	30.18
16.40	22.46	32.38
17.50	23.01	34.58
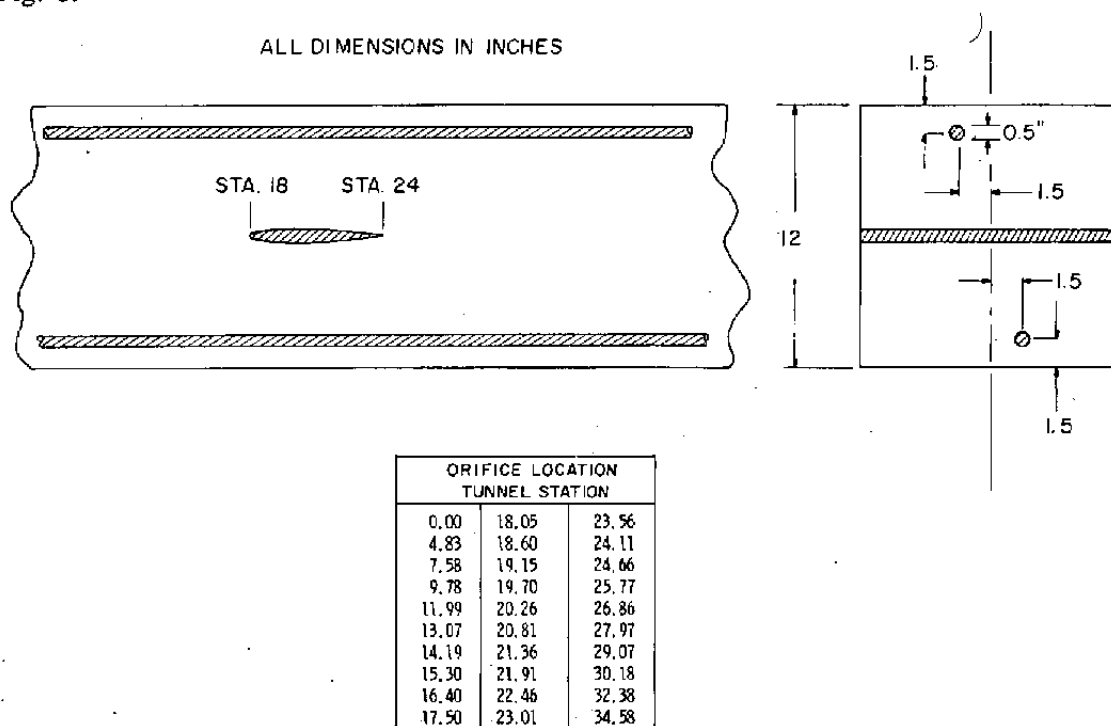
Figure 6. Static pressure pipe.

Measurement of the flow-angle distribution at S was accomplished with an array of fixed-location, differential-pressure yawmeter probes. A two-tube type of yawmeter (generally referred to as a Conrad probe) was the design selected since it provides: (1) a convenient design for miniaturization to minimize flow disturbances, (2) adequate sensitivity that is relatively free of Mach number and Reynolds number effects (see Ref. 21), and (3) orifices that are close together for nearly point measurements of flow angularity. The details of the probe plus a table of the probe locations are shown in Fig. 7.

The flow angularity probes were individually calibrated to determine their sensitivity ($\Delta\theta/\Delta P$) and were accurate to within ±0.1 deg. The probes were then installed in the tunnel test section. The individual probe calibration offset, or the indicated pressure differential for

13

PROBE TIP LOCATIONS

TUNNEL STATION	DISTANCE FROM SIDEWALL
3.78	2.80
10.39	3.37
12.59	4.51
14.80	5.08
16.45	5.65
17.55	6.23
19.20	2.23
20.86	2.80
22.51	3.37
24.16	4.51
26.37	5.08
28.57	5.65
32.98	6.23

ALL DIMENSIONS IN INCHES
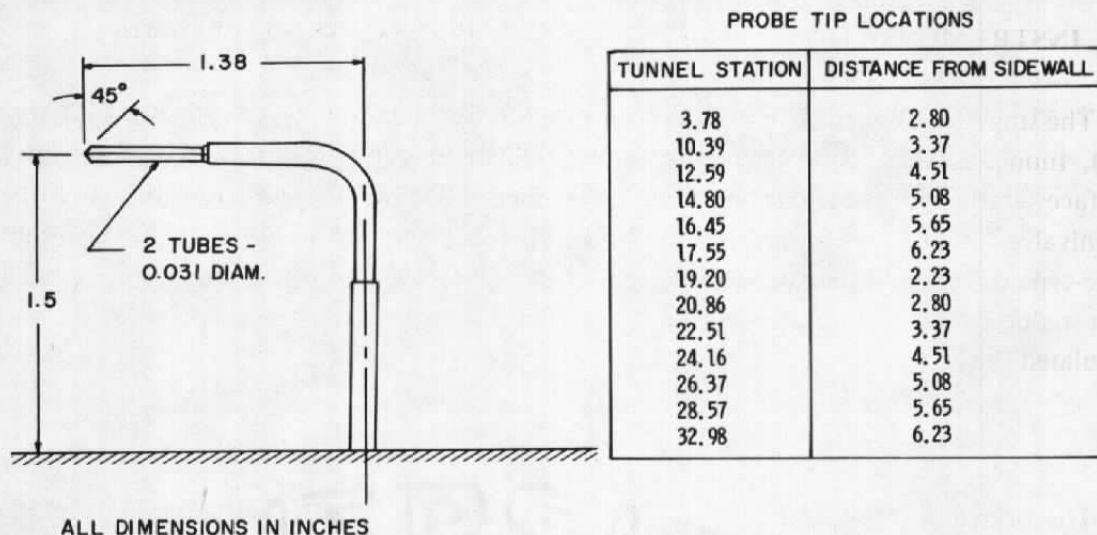
Figure 7. Flow-angle probe.

zero angle, was determined as follows. The perforated walls were closed to yield solid surfaces. The Mach number was established in the test section, and the flow was assumed parallel to the tunnel centerline. Thus, a reference angle was defined for each probe. Subsequent probe measurements were corrected accordingly.

The test section configuration for the experiments is shown in Fig. 8.
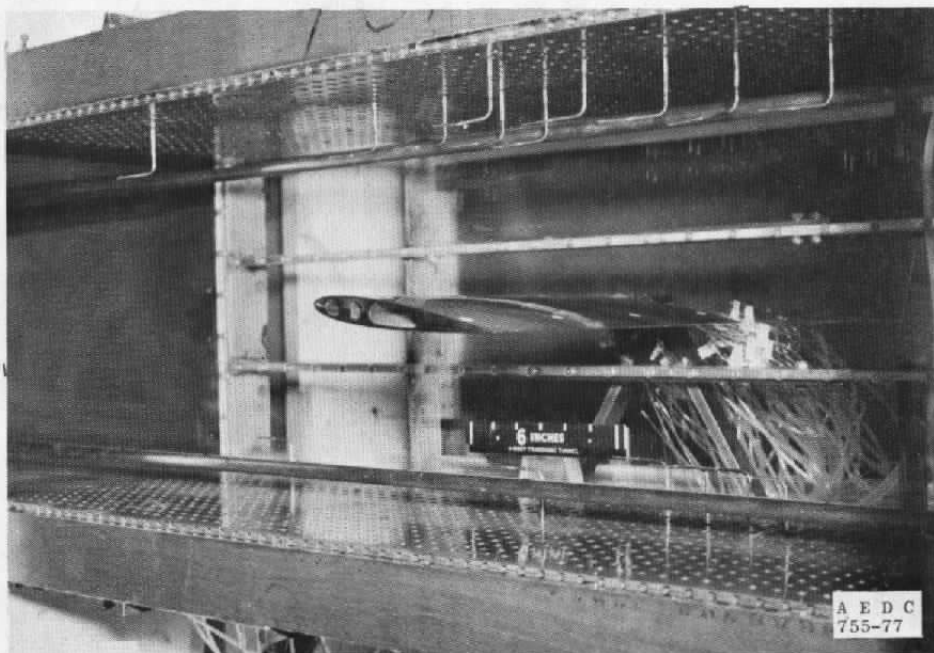
Figure 8. Adaptive-wall test section configuration.

3.5 INSTRUMENTATION

The standard Tunnel 1T instrumentation was used to measure plenum chamber pressure (P_c), tunnel total pressure (P_T), and tunnel total temperature (T_o). Model and control surface static pressure distributions were measured by 15-psid transducers using Scanivalves®. The pressure differential of each flow-angle sensor was measured by a strain-gage-type differential pressure transducer. The data were recorded by a computer system that reduced the raw data to engineering units, computed pertinent parameters, and tabulated the results.

4.0 COMPUTATIONAL METHODS

The principal theoretical aspect of the adaptive-wall method is the evaluation of the functional relationships that satisfy the conditions for unconfined flow in the region exterior to S (as shown in Fig. 9). This requires the solution of the flow field exterior to the interface with the distribution of one of the measured flow variables prescribed as the boundary condition. Since the region exterior to S contains no immersed bodies (and, hence, no boundary layers) and since S is presumed sufficiently removed from the experimental model so that disturbances from the model have weakened, the application of inviscid, small-disturbance theory to the exterior region appears justified.
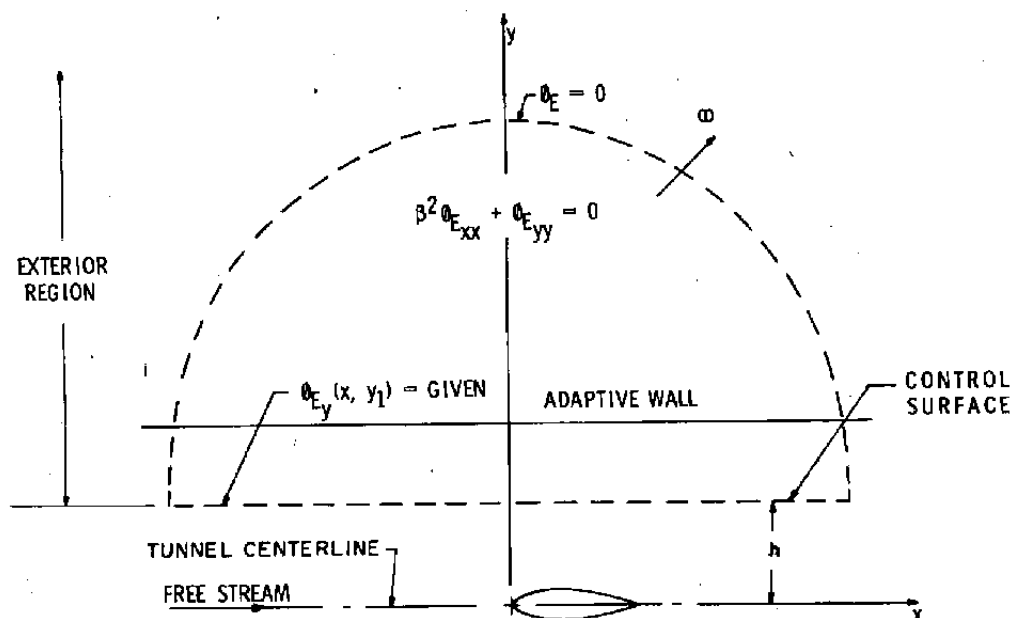

Figure 9. Boundary-value problem of exterior unconfined region.

Consistent with the small-disturbance approximation, working in terms of the nondimensional disturbance velocity components streamwise and normal to the reference surface, S, respectively u and v, was found convenient. Since static pressure and flow-angle distributions were measured at S, the linear approximations $u = -C_p/2$ and $v = \theta$ were utilized. Some preliminary studies of the adaptive-wall concept made it apparent that it would be advantageous to use v as the boundary condition in the external region and to use u as the parameter to adjust the tunnel boundaries. The primary reason for assigning these functions to u and v is that the flow in the tunnel appears to be more sensitive to changes in pressure (or u) than to changes in flow direction (or v). Details of the relative effectiveness of u and v are given in Ref. 22.

In the present study, three techniques were used to evaluate the requisite functional relationships at the interface S. The first technique is based on the Prandtl-Glauert form of the linear small-disturbance equations for subcritical flow at the interface. From the boundary value problem illustrated in Fig. 9, it can be directly determined that the external region solution (Ref. 13) for the axial perturbation velocity, u_E, based on the measured flow-angle distribution, v_T, is

$$u_E(X, \pm h) = \frac{-1}{\pi\beta} \oint \frac{v_T(\xi, \pm h)}{\xi - X} \, d\xi \tag{1}$$

where $y = \pm h$ are the reference surfaces, S, for the two-dimensional problem and $\beta = \sqrt{1 - M_\infty^2}$. Equation (1) must be evaluated in the sense of the Cauchy principal value. For applications, the singularity in Eq. (1) is removed, and the integral evaluated by simple quadrature of the curve fit values of the measured v_T.

The second technique is also based on linearized small-disturbance theory. However, instead of calculating the external region flow field to iteratively adjust the tunnel boundaries, criteria have been developed for determining interference-free conditions directly from the flow variables measured at S. Reference 13 details the development of the one-step convergence formula for a nonlifting airfoil. The criteria have been extended to a lifting airfoil (Ref. 23), and the resulting one-step formulas are

$$u_\infty(X, \pm h) = \frac{1}{2} u_T(X, \pm h) - \frac{\beta h}{\pi} \int_{-\infty}^{\infty} \frac{u_T(\xi, \pm h)}{K(\xi - X)} \, d\xi$$

$$\pm \frac{1}{2\pi\beta} \int_{-\infty}^{\infty} \frac{v_T(\xi, \pm h)}{\xi - X} \, d\xi \pm \frac{1}{2\pi\beta} \int_{-\infty}^{\infty} \frac{v_T(\xi, \pm h)(\xi - X) \, d\xi}{K(\xi - X)} \tag{2}$$

and

$$v_\infty (X, \pm h) = \frac{1}{2} v_T(X, \pm h) - \frac{\beta h}{\pi} \int_{-\infty}^{\infty} \frac{v_T(\xi, \pm h)}{K(\xi - X)} d\xi$$

$$\pm \frac{\beta}{2\pi} \int_{-\infty}^{\infty} \frac{u_T(\xi, \pm h)}{\xi - X} d\xi \pm \frac{\beta}{2\pi} \int_{-\infty}^{\infty} \frac{u_T(\xi, \pm h)(\xi - X) d\xi}{K(\xi - X)} \tag{3}$$

where

$$K(\xi - X) = (2\beta h)^2 + (\xi - X)^2 \tag{4}$$

Once u_T and v_T are determined at the measuring plane, then the interference-free conditions can be determined directly from Eqs. (2) and (3) as long as the exterior region remains subcritical.

If supercritical flow exists near the measuring surface, S, it is necessary to account for discontinuities in the flow field with a nonlinear theory. In the present study, a mixed-operator finite-difference scheme was used to solve the transonic small-disturbance equation

$$\left[K - (\gamma + 1) \phi_X \right] \phi_{XX} + \phi_{\bar{y}\bar{y}} = 0 \tag{5}$$

where the transonic similarity parameter, K, is defined by

$$K = \frac{\beta^2}{M_\infty t^{2/3}} \tag{6}$$

and the transformed y coordinate is

$$\bar{y} = t^{1/3} M_\infty y \tag{7}$$

where t is the thickness ratio of the airfoil.

Equation (5) was approximated in the exterior region on a 150 by 80 uniform grid mesh. The measured flow angle, v_T, was smoothed and curve fit to provide the boundary condition at y = 0. Uniform flow, $C_p = 0$, was used as the boundary condition on the other three boundaries of the computational domain.

As discussed in Ref. 13, the average of the measured velocity, u_T, and the calculated velocity, u_E, provides a good approximation to conditions for unconfined flow. In addition, as convergence to unconfined flow is approached, the result of the one-step formula, u_∞, should be identical to the exterior solution, u_E. During the test program, u_∞, derived from the one-step formula [Eq. (2)], was used to adjust the tunnel boundary as long as the flow at the control surface remained subcritical. At higher Mach numbers, the average of the measured value, u_T, and external solution, u_E, was used as the criterion for adjusting the tunnel boundaries. At converged conditions, u_∞ and u_E typically agreed.

5.0 TESTING PROCEDURE

The wind tunnel top and bottom test section walls were aligned parallel and level. The two-dimensional NACA 0012 wing model, which spanned the tunnel test section, was adjusted to within ±0.1 deg of the desired angle of attack, defined as the angle relative to the tunnel horizontal axis. All data were obtained with natural boundary-layer transition on the wing model. The test Reynolds number varied from nominally 4×10^6 at Mach number 0.65 to 4.8×10^6 at Mach number 0.85.

The test Mach number was defined and input to the online data reduction program. The pressure on the model surface and the adaptive-wall control surface was converted to coefficient form based on the defined Mach number. A flow was established in the test section at the pressure ratio specified by the tunnel empty calibration. The actual flow conditions were obtained by adjusting the plenum pressure and tunnel pressure ratio to yield a control surface pressure coefficient equal to zero far upstream for the 0th iteration, or equal to the desired value if different from zero, for subsequent iterations as determined by the exterior computations.

The LVHA walls were calibrated, accounting for their crossflow characteristics for discrete values of hole inclination and were locally adjusted for the adaptive-wall experiments using the calibration results. The local crossflow characteristics were altered by changing the local hole angle to reduce the difference between the measured control surface pressure distribution and that required by the external computations.

The wall hole angle was adjusted manually. For expediency, when test conditions were changed, the walls were not always returned to a uniform distribution of hole angle as for the 0th iteration.

6.0 RESULTS AND DISCUSSION

6.1 LONGITUDINALLY VARIABLE HOLE ANGLE WALL

A free-stream Mach number of 0.65 and a model angle of attack of 0 deg were the test conditions for the initial experiments since the flow along the control surface would be subsonic. The pressure distribution along the control surface for a uniform hole angle of 0 deg (normal holes) is shown in Fig. 10. Also shown in Fig. 10 is the required pressure distribution for unconfined flow as computed from the measured velocity distributions along the control surface using the one-step formula. The measured pressure distribution for the initial run conditions, or 0th iteration, are essentially in agreement with the unconfined-flow requirements.
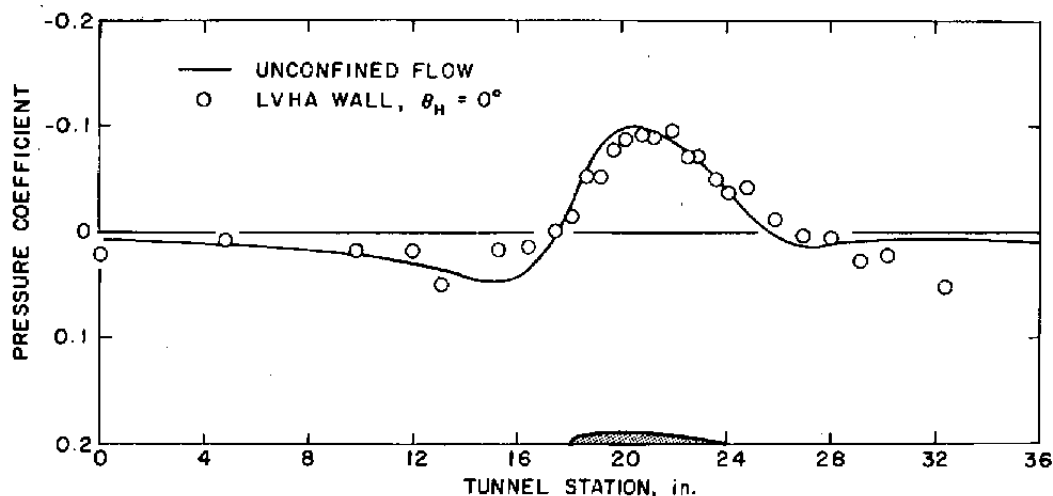

Figure 10. Control surface pressure distribution, $M_\infty = 0.65$ and $\alpha = 0$ deg.

The model surface pressure distribution for the above case is shown in Fig. 11 along with data obtained in the Calspan 8-foot Transonic Wind Tunnel for a similar model (Ref. 18). The Calspan data are assumed to be free from tunnel wall interference. As Fig. 11 demonstrates, the data nearly agree. The suppression of the Calspan model pressure distribution between the ten- and twenty-percent-chord station is believed to have been caused by the transition strip at the 10-percent-chord location. The Calspan data also exhibit separation over the aft ten percent of the chord, whereas the present data indicate attached flow at the trailing edge. It should be noted that the Calspan experiments were conducted at a chord Reynolds number of 10^6, whereas the present experiments were conducted at a nominal chord Reynolds number of 2.0×10^6.
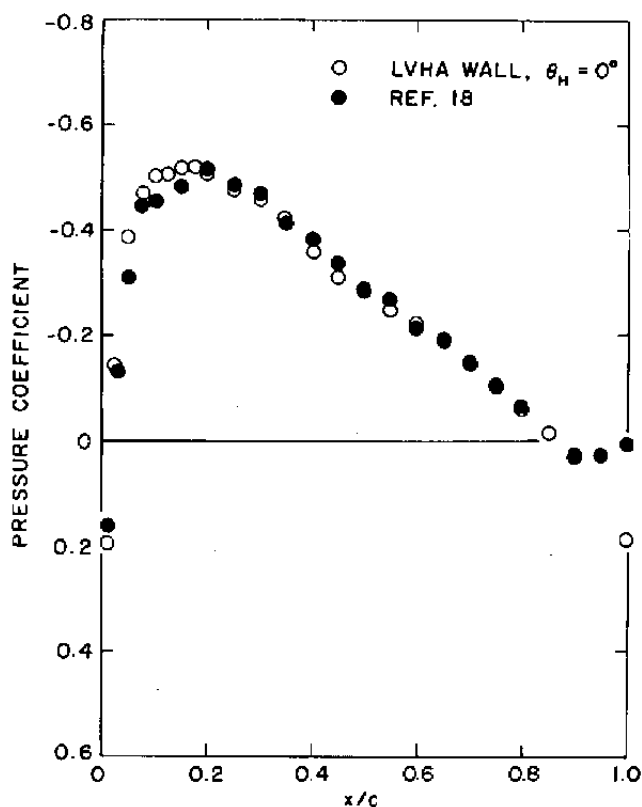
19

Figure 11. Model surface pressure distribution, $M_\infty = 0.65$ and $\alpha = 0$ deg.

It is interesting to note that no wall adjustments were required at these test conditions. References 24 and 25 indicate the effect of large-blockage models on the plenum pressure calibration. The plenum calibration is a standardized method of defining the test section Mach number by relating an average test section centerline Mach number to corresponding values of the plenum chamber pressure and pressure ratio across the test section. The procedure of predefining the Mach number and adjusting the upstream test section conditions correspondingly, eliminates most of the solid-blockage effects. This will be demonstrated more clearly in Section 6.2.

To investigate the adaptive-wall concept for supercritical flow, experiments were also performed for a free-stream Mach number of 0.8. At $M_\infty = 0.8$, the flow was expected to be supercritical at the airfoil surface but subcritical at the measurement plane. A measurement of the pressure distribution at the control surface for the initial wall configuration is shown in Fig. 12. Comparison with the pressure distributions calculated using the corresponding measured flow angles (Fig. 12) shows that the particular LVHA wall configuration was too closed in the region over the model. The indicated peak level for the pressure coefficient
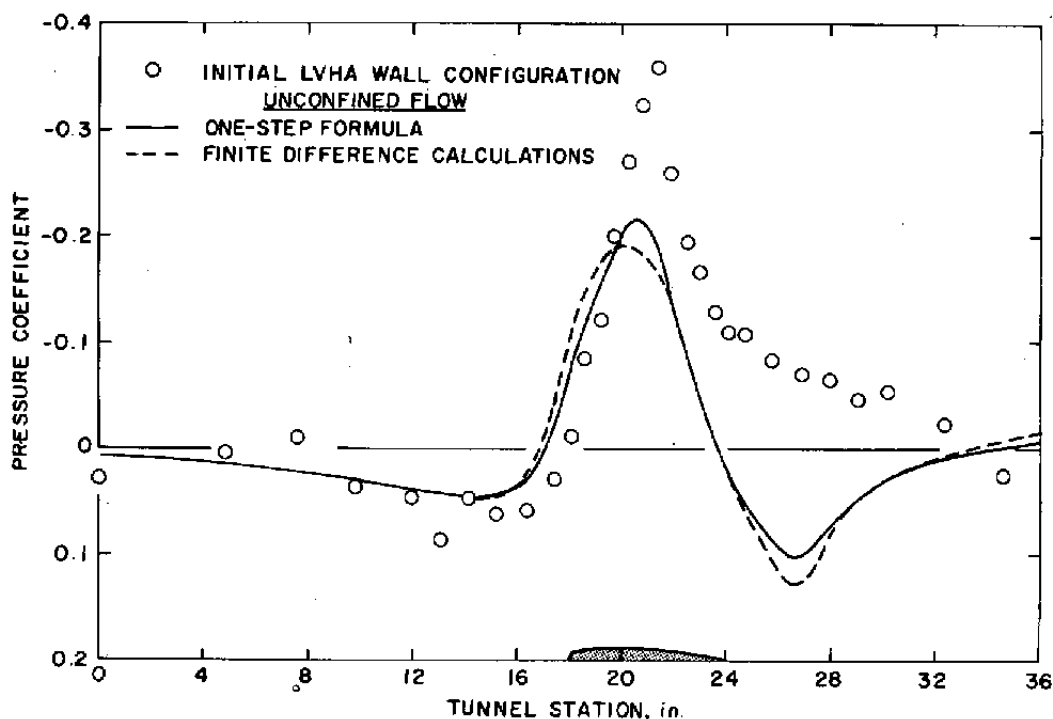
Figure 12. Control surface pressure distribution, $M_\infty = 0.8$ and
$a = 0$ deg.

from either the computed C_{p_∞} or the average of the measured values and exterior computed values $[C_{p_E} + C_{p_T})/2]$ is nominally -0.23. This nominal value was obtained by adjusting the LVHA wall and the suction through the wall. The resulting pressure distribution is shown in Fig. 13. The corresponding computed values of C_{p_∞} and C_{p_E} indicate that unconfined flow has been achieved. It should be noted that, at convergence, C_{p_∞} and C_{p_E} are essentially equal, as expected from theoretical considerations.

The distribution of the measured pressure coefficient shown in Fig. 13 was obtained with some adjustment also to the pressure ratio across the test section (TPR). During this test phase, no clear criterion was developed for determining the required pressure ratio from the control surface information. Therefore, model information — the recompression shock location — was employed as the adjustment criteron. This criterion for TPR adjustment was deemed acceptable for this phase of the technique development for demonstrating the extent of the available boundary control. A comprehensive criterion for adjusting pressure ratio remains to be developed.

The pressure coefficient distributions on the airfoil at $M_\infty = 0.8$ for both the initial wall setting and the converged wall setting are shown in Fig. 14. Comparison with the Calspan 8-ft Tunnel data shows that the converged wall setting has produced interference-free flow on the model.
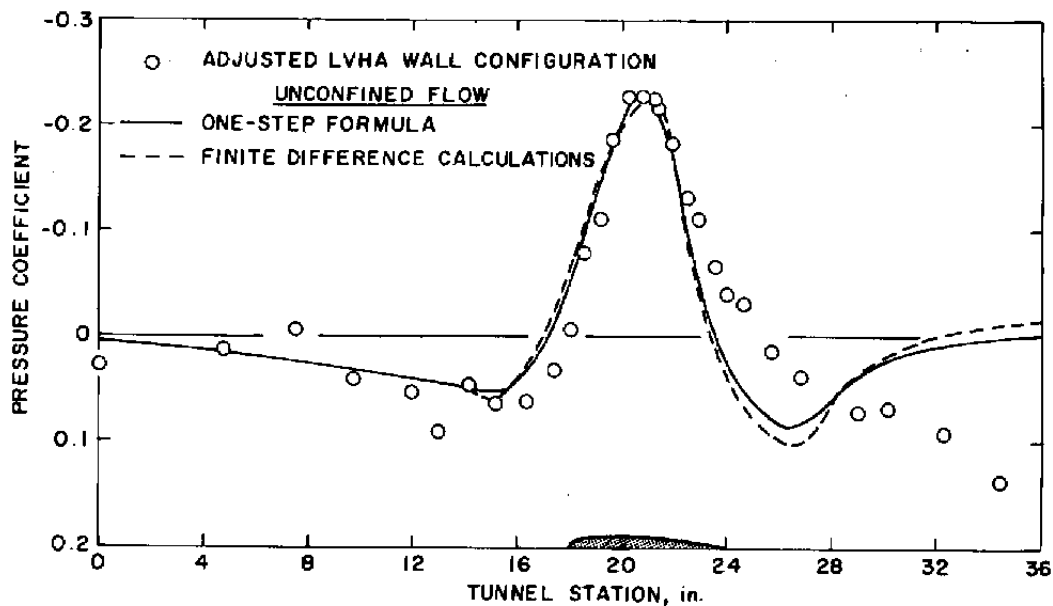
21

Figure 13. Adjusted wall control surface pressure distribution,
$M_\infty = 0.8$ and $\alpha = 0$ deg.

The corresponding flow angles at the control surface used in the calculations for Figs. 13 and 14 are shown in Fig. 15. Their respective results for the one-step formula for flow angle are also shown in Fig. 15. It is interesting to note that the flow angle changed almost insignificantly during the wall adjustment, although large changes were made in the pressure coefficient distribution. This concurs with the Calspan findings (Ref. 23) that the pressure coefficient is a much more sensitive indicator for adjusting the tunnel boundaries. Also, the unconfined flow angles calculated from Eq. (3) agree well with these measures except in the region downstream where variations are caused by adjustments of the tunnel pressure ratio. These data are typical for flow-angle variations with wall adjustments experienced throughout the experimental program.

An extension of the demonstration to the condition of $M_\infty = 0.8$ and $\alpha = 1$ deg, where flow conditions are asymmetric about the tunnel centerline, yields the results shown in Figs. 16 through 19. Figure 16 shows the measured pressure distribution at the control surface for a standard tunnel configuration of 4-percent uniformly distributed porosity on the top and bottom walls along with the corresponding values of C_{p_∞}. The model surface pressure distribution is shown in Fig. 17. The control surface pressure distribution for the LVHA wall adjusted to give the best possible agreement with the computed unconfined values through variable hole angle distribution, plenum suction, and pressure ratio is shown in Fig. 18. The pressure distributions for both upper and lower control surfaces are in agreement with the required distribution except for the area just downstream of the model between tunnel stations 23 to 28 in.
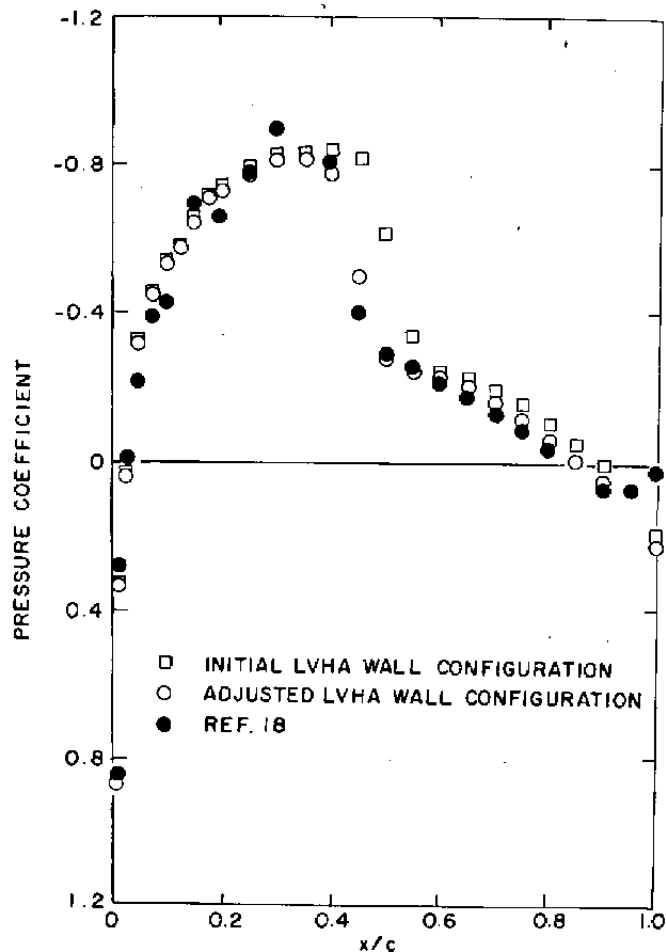
Figure 14. Model surface pressure distribution, $M_\infty = 0.8$ and $\alpha = 0$ deg.

The model data of Fig. 19 agree well with the Calspan results for interference-free conditions. The observed area of disagreement of the pressure distributions at the control surface apparently has little effect at the model surface.

Several observations were made during the experiments with the LVHA walls. First, the solid-blockage effects of the large model could be eliminated by adjusting the upstream Mach number in the test section. Second, only small longitudinal variations of the hole angle distribution were required to make the control surface pressure distribution accord with that required. Longitudinal hole angle variations usually had minimal effects on the control surface distribution. It should be recalled that the entire plenum-side surfaces of the upper and lower walls face a common plenum at a spatially constant pressure. Third, and most important, the dominant features of the control surface distribution were the value and location of the minimum pressure, or peak, in the vicinity of the model. The observation

that the peak pressure match was a primary factor in minimizing interference on the model suggested experiments with globally variable-porosity walls like those installed in the AEDC Aerodynamic Wind Tunnel (4T). When the experimental value of the peak pressure was matched to that required for unconfined flow, the model data compared well with the interference-free results even though differences existed between the measured and computed control surface pressure distributions just upstream and downstream of the model.

Lack of control in the region near the model leading edge, where there is considerable outflow through the wall into the plenum, and also in the region near the trailing edge, where there is considerable inflow through the wall into the test section, is believed responsible for the failure to duplicate the required control surface pressure distribution. One method to possibly increase the boundary control in these local regions is to insert two subplena with independent pressure controls. The subplena would be positioned so that one would control the inflow and the other the outflow region.
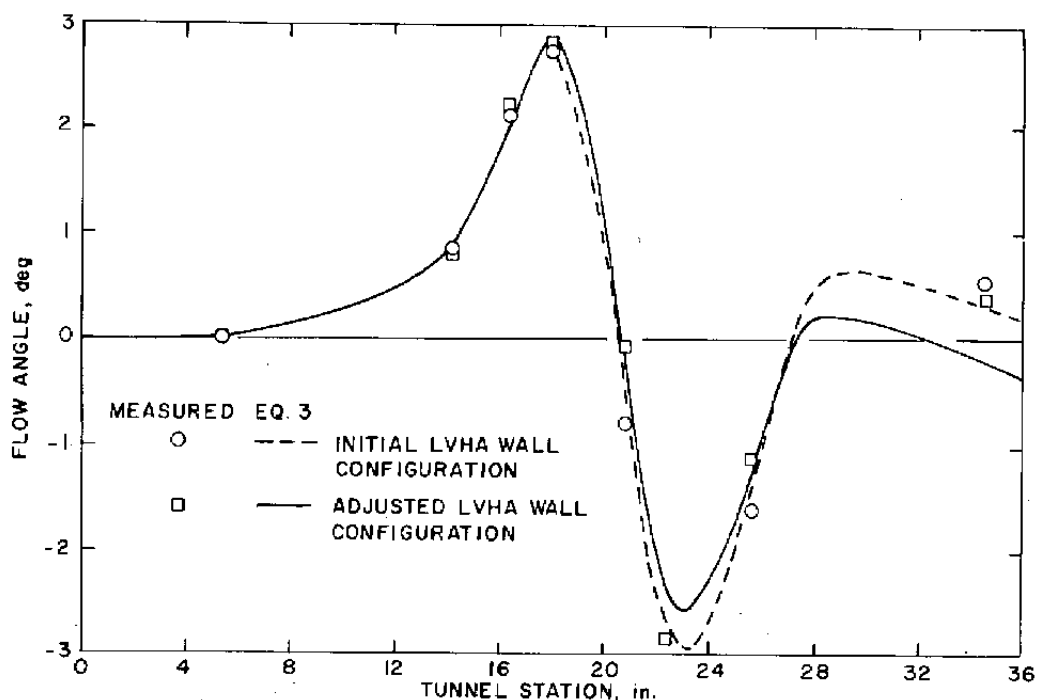

Figure 15. Flow-angle distribution at the control surface, $M_\infty = 0.8$ and $\alpha = 0$ deg.
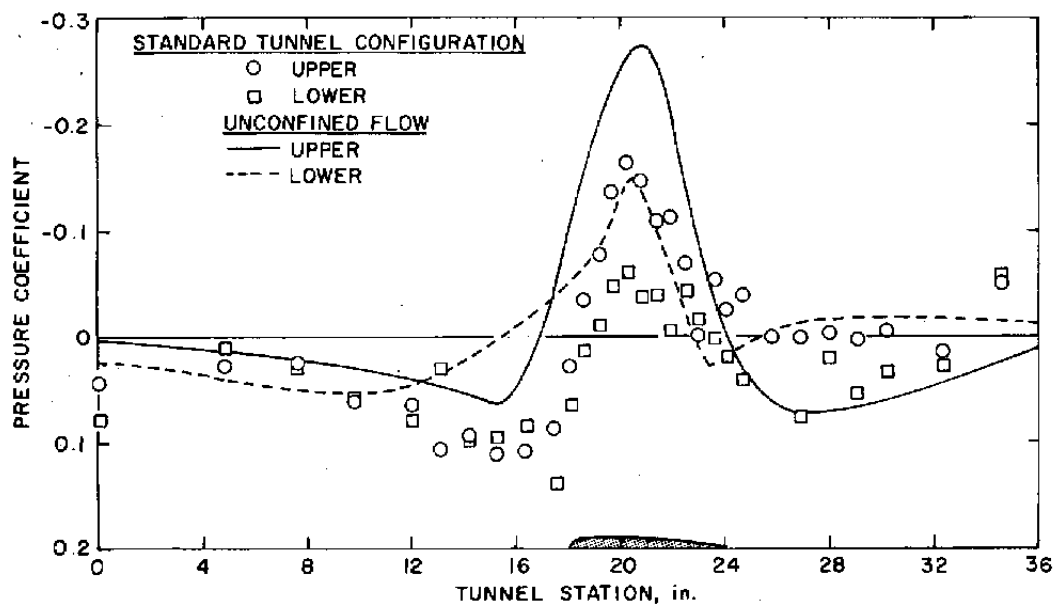
Figure 16. Control surface pressure distribution for the standard tunnel configuration, $M_\infty = 0.8$ and $a = 1$ deg.
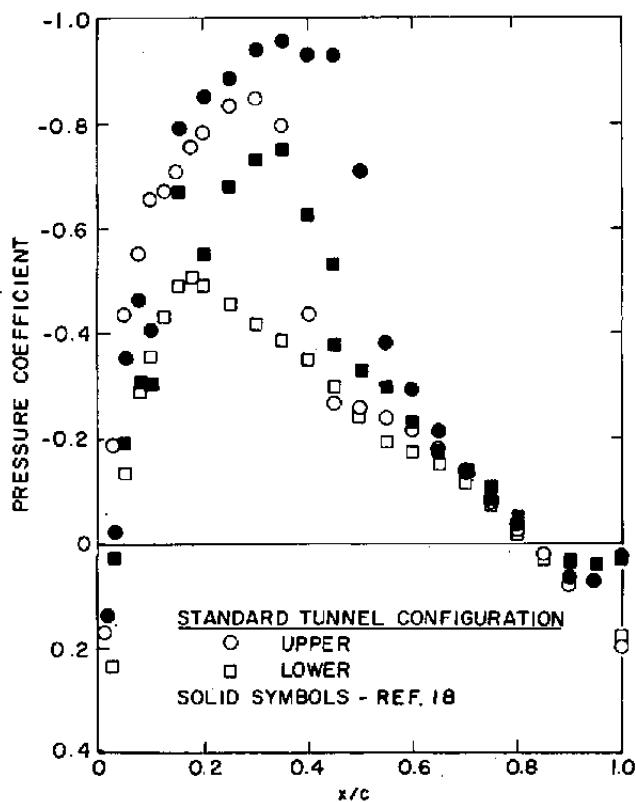

Figure 17. Model surface pressure distribution for the standard tunnel configuration, $M_\infty = 0.8$ and $a = 1$ deg.
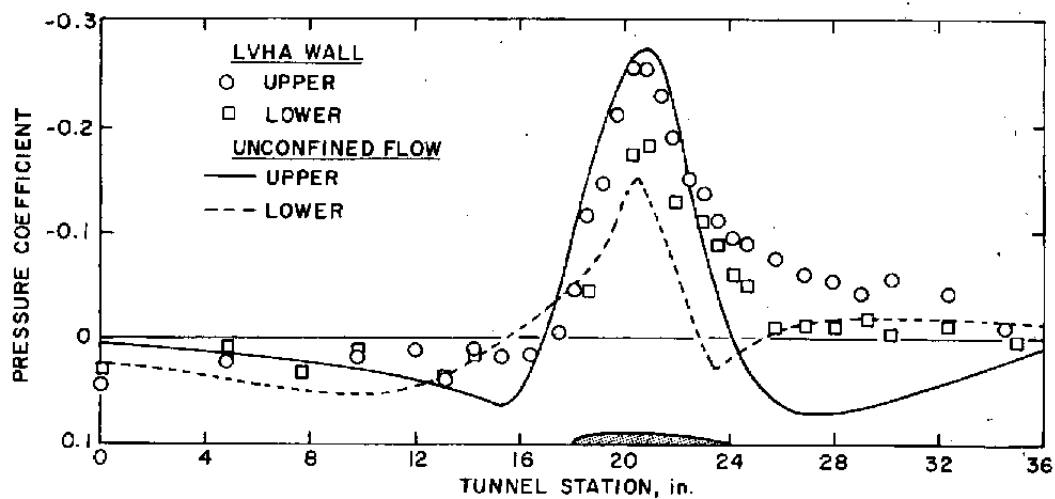
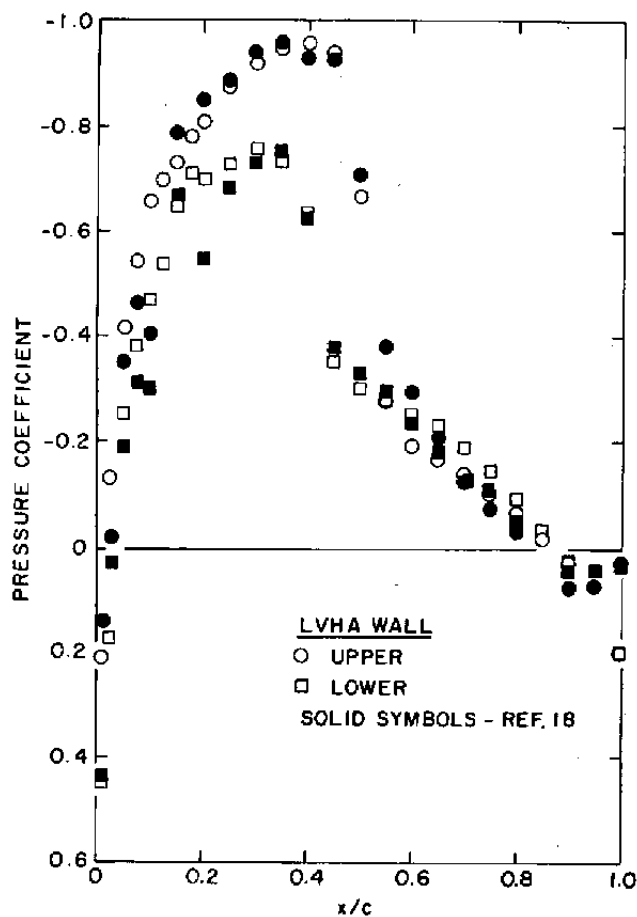Figure 18. Control surface pressure distribution, $M_\infty = 0.8$ and $a = 1$ deg.

Figure 19. Model surface pressure distribution, $M_\infty = 0.8$ and $a = 1$ deg.

6.2 VARIABLE-POROSITY WALLS

As noted for the LVHA experiments, the wall interference level is characterized more by global features (specifically the minimum pressure coefficient at the control surface) than by the detailed distribution of the velocity components at the control surface. This observation led to the hypothesis that adaptive-wall technology could be used to establish criteria for adjusting the porosity and/or plenum suction of existing conventional variable-porosity walls to minimize wall interference. Hence, an experiment was designed using the variable-porosity wall as an adaptive wall.

For this "proof of concept" experiment, the measurement of the second flow variable — the flow angle — at the control surface was dispensed with for expediency. Instead, the pressure coefficient distribution for minimum-interference testing was obtained from the LVHA experiments. The aim of the experiment was to establish that by globally matching the interference-free pressure distributions, a conventional variable-porosity wall could be used to significantly reduce wall interference.

The strategy employed in the variable-porosity wall experiment was to vary wall porosity and plenum suction until the minimum pressure coefficient measured at the control surface was equal to that for the free-air distribution from the LVHA wall test phase. The location of the minimum pressure was dictated by the model flow field. The effectiveness of this strategy is indicated in Figs. 20 through 23 for $M_\infty = 0.8$ and $\alpha = 0$ deg. The control surface
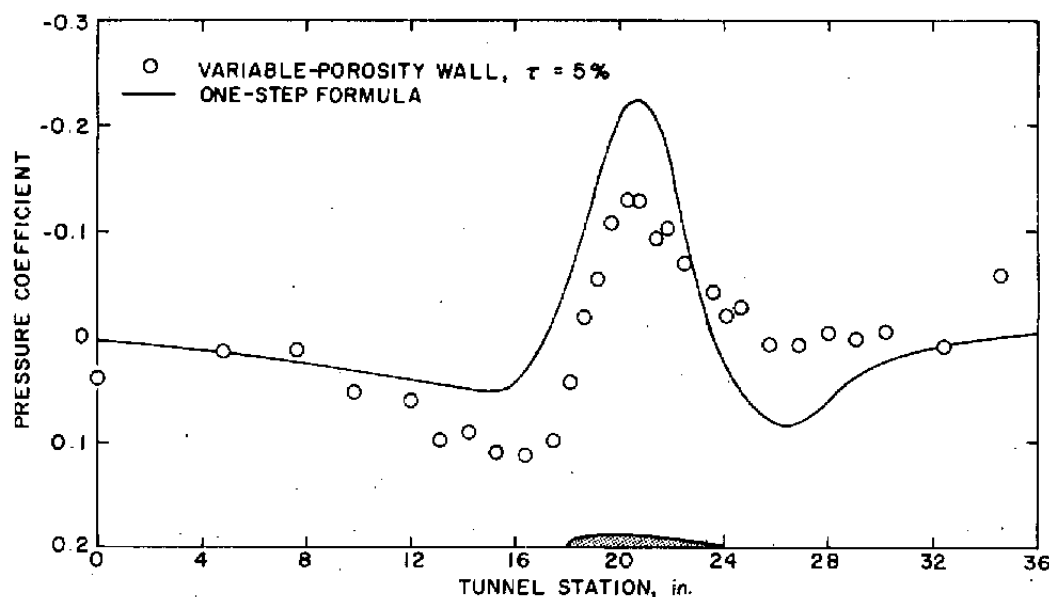

Figure 20. Control surface pressure distribution for the standard tunnel configuration, $M_\infty = 0.8$ and $\alpha = 0$ deg.

27

and model surface pressure distributions for the standard tunnel configuration of 5-percent porosity are shown, respectively, in Figs. 20 and 21. Since the walls were not automated, discrete values of porosity of 3, 4, and 5 percent were set, and the plenum suction was adjusted to obtain the best match of the peak value on the unconfined-flow distribution. The results are shown in Fig. 22. For this test condition, the value of the peak pressure was approximated for both 4- and 5-percent porosity. Comparison of the corresponding pressure distribution on the wing surface (Fig. 23) with interference-free data (Ref. 18) shows that the data for wall porosities of both 4 and 5 percent are in reasonable agreement with those from Ref. 18.
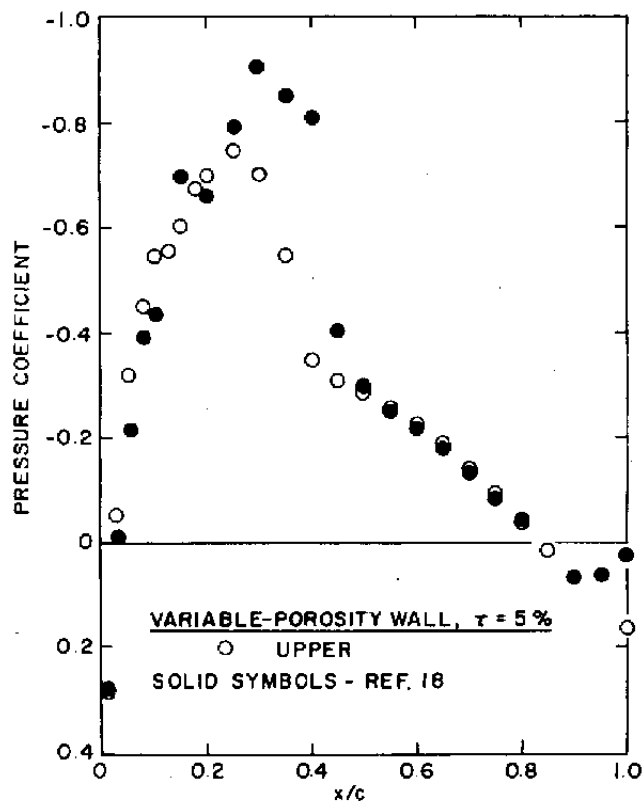

Figure 21. Model surface pressure distribution for the standard tunnel configuration, $M_\infty = 0.8$ and $\alpha = 0$ deg.

It is significant that the improvement in the control surface pressure distribution from Fig. 20 to Fig. 22 resulted primarily from plenum suction adjustment. This was essentially a Mach number adjustment to compensate for the effects of the large-blockage model on the tunnel empty plenum calibration. The effect of Mach number adjustment can be seen in Figs. 24 and 25 for a wall porosity of 5 percent at $M_\infty = 0.8$ and $\alpha = 0$ deg. As seen in Fig. 24, a wide disparity exists between the control surface pressure distribution for unconfined flow and the distribution measured with the tunnel Mach number set by the plenum

calibration. This disparity indicates the significant effect that the large model blockage has on the tunnel empty plenum calibration previously noted in Section 6.1. The Mach number set by the calibration is too low; consequently, the supercritical region on the airfoil appears to be suppressed (Fig. 24) because of the Mach number error.
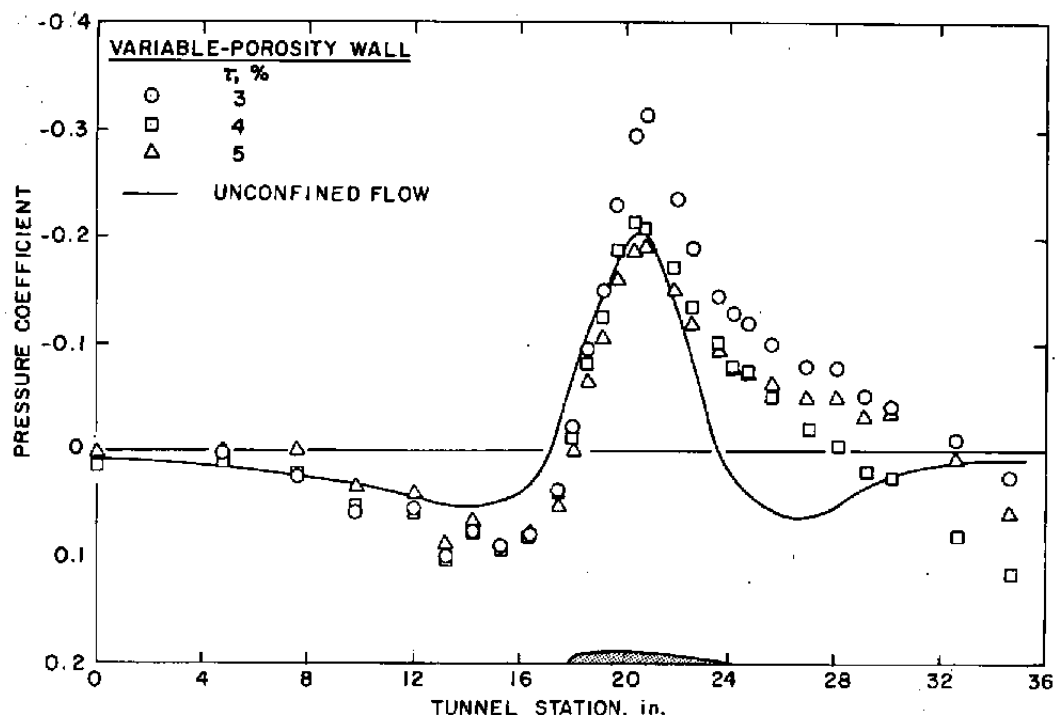

Figure 22. Control surface pressure distribution, M_∞ = 0.8 and a = 0 deg.

By adjusting plenum suction (i.e., by increasing the Mach number) to match the measured pressure with the peak of the free-air pressure distribution, interference was significantly reduced (Fig. 25). Again, the results could be improved by decreasing the porosity (Fig. 22) for the same test conditions. The ideal porosity for this test condition is apparently between 4 and 5 percent. Figures 21 through 24 verify that wall interference can be significantly reduced in a conventional variable-porosity wall tunnel by globally matching the free-air control-surface distributions that can be predicted, according to the adaptive-wall concept, by using flow-field measurements and exterior region calculations.

Subsonic wall-interference theory indicates that lift, blockage, and streamline curvature effects cannot be simultaneously eliminated with an equal value of porosity for all walls. However, for differential porosity between top and bottom walls, subsonic theory does indicate that lift and blockage can be reduced simultaneously. Furthermore, experimental evidence (Ref. 26) indicates that individual walls do have different resistances to the tunnel

flow with a lifting model. It would be beneficial, therefore, to use a technique of differentially adjusting porosity in a variable-porosity wall tunnel. Heretofore, no rational method for setting differential porosity was available, and all testing in variable-porosity wall tunnels has been done with the same porosity on each wall. In the present experiment, however, the adaptive-wall technology provided a rational method for setting differential porosity as discussed below.
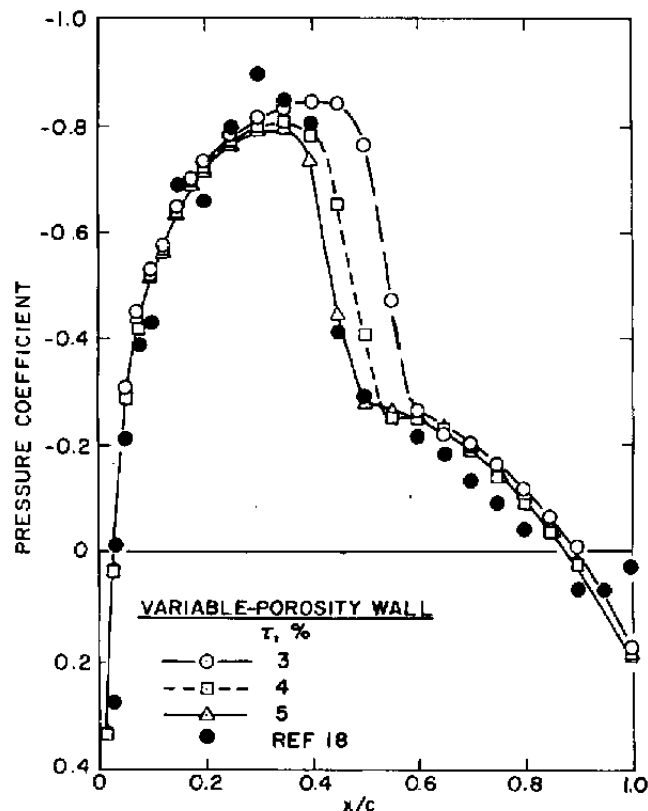

Figure 23. Model surface pressure distribution, M$_\infty$ = 0.8 and
        a = 0 deg.

The control surface and model surface pressure distributions for uniform top and bottom wall porosity of 4 percent and the tunnel calibrated parameters at M$_\infty$ = 0.8 and α = 1 deg are shown in Figs. 16 and 17, respectively. In Fig. 26, plenum suction was adjusted until the measured pressure matched the upper control surface free-air peak value. Figures 22 and 23 show that 4-percent porosity was effective in minimizing blockage interference at α = 0 deg. However, at α = 1 deg for equal top- and bottom-wall porosity (Fig. 26), the peaks of the pressure distributions were not simultaneously matched at both the top and bottom control surfaces. For the case shown in Fig. 26, the disparity between the unconfined and measured distributions on the bottom control surface suggests that the bottom wall is too open since the measured pressure is more positive than that
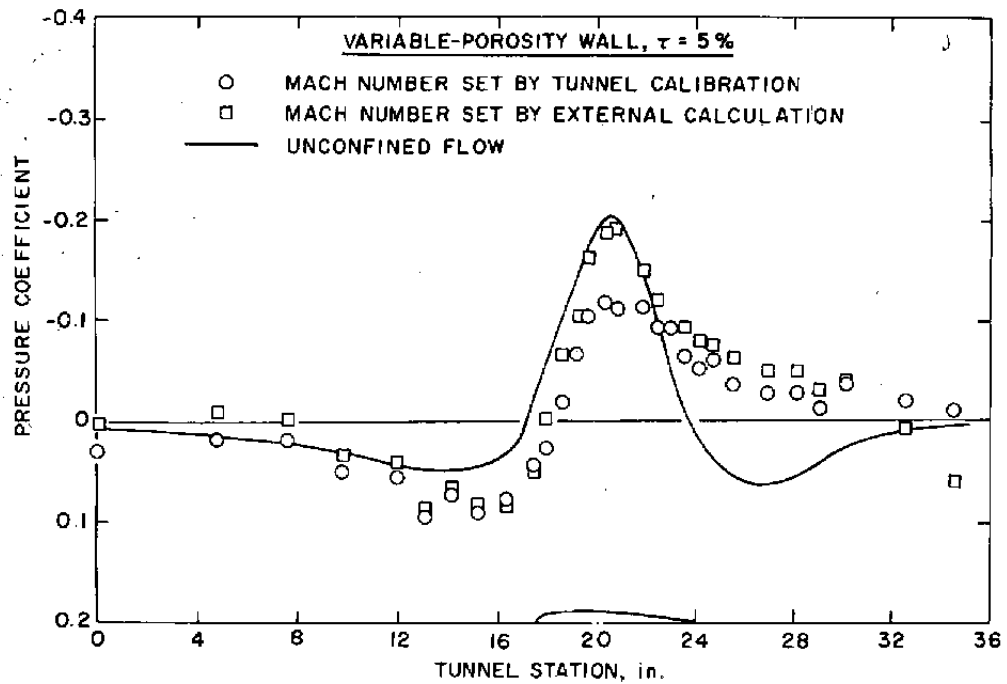
30

Figure 24. Effect of model blockage on the tunnel calibration at the control surface, $M_\infty = 0.8$ and $\alpha = 0$ deg.
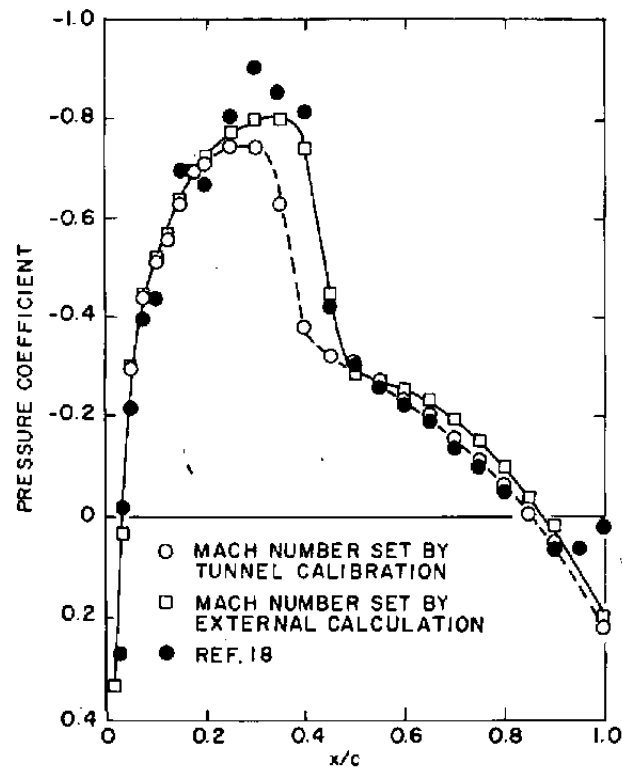

Figure 25. Effect of model blockage on the tunnel calibration at the model surface, $M_\infty = 0.8$ and $\alpha = 0$ deg.

corresponding to free air. Examination of the pressure distributions on the airfoil (Fig. 27) shows the shock wave on the lower surface to be displaced forward correspondingly.

Therefore, to properly simulate the flow over the airfoil at angle of attack requires a differential setting of porosity. Based on the results shown in Figs. 26 and 27, it is logical to presume that the porosity on the lower wall should be decreased. At the same time, to minimize the effects of blockage (a function of the overall average porosity), the upper-wall porosity should be increased. Figures 28 and 29 present results for experiments incorporating a porosity setting of 5 percent on the upper wall and 3 percent on the lower wall. Figure 29 shows that both peaks of the pressure distribution were matched with the differential-porosity settings. Inspection of Fig. 29 reveals that the effects of the tunnel walls on lift and blockage have, indeed, been significantly reduced since the model data are in good agreement with the interference-free results from Ref. 18.

Figure 26. Control surface pressure distribution for uniform top and bottom wall porosity, M_∞ = 0.8 and a = 1 deg.

Figure 27. Model surface pressure distribution for uniform top and
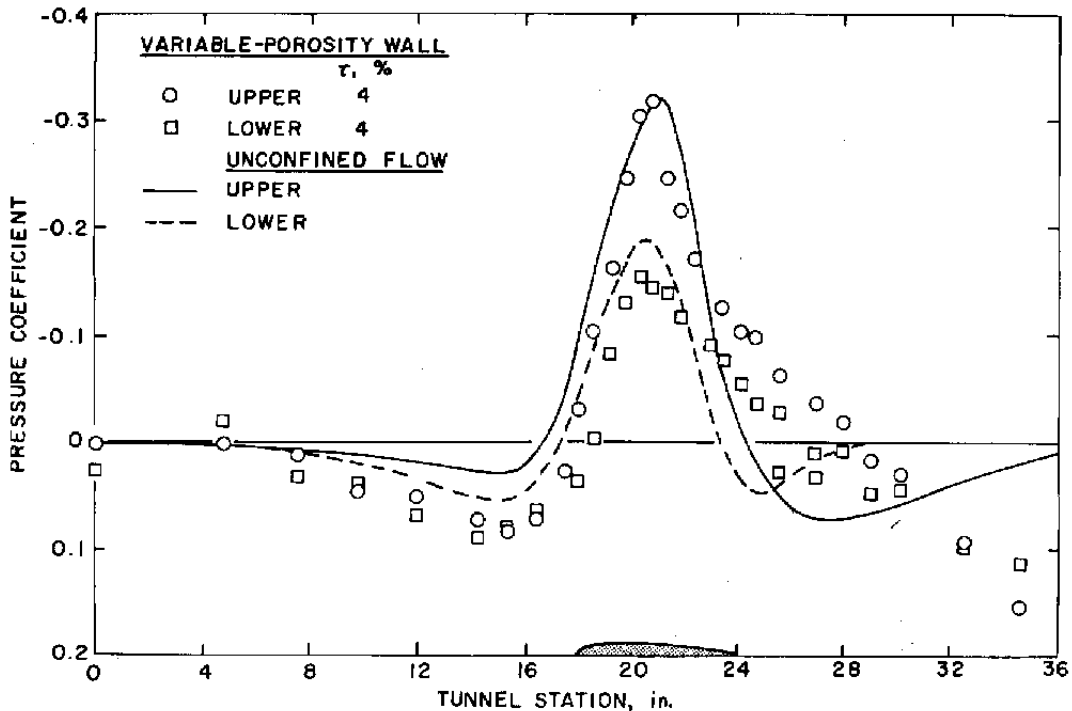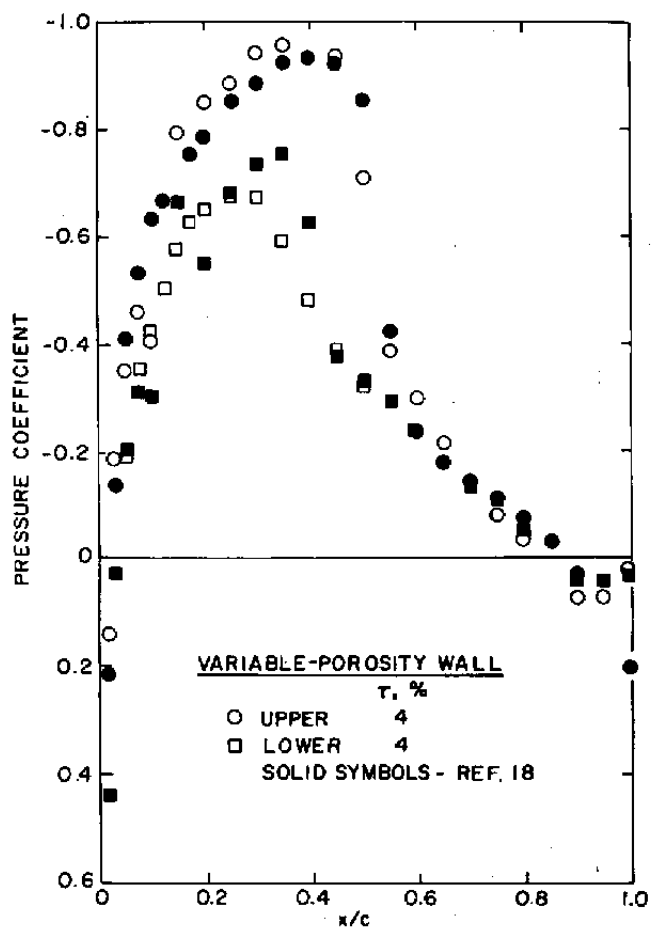bottom wall porosity, $M_\infty = 0.8$ and $a = 1$ deg.
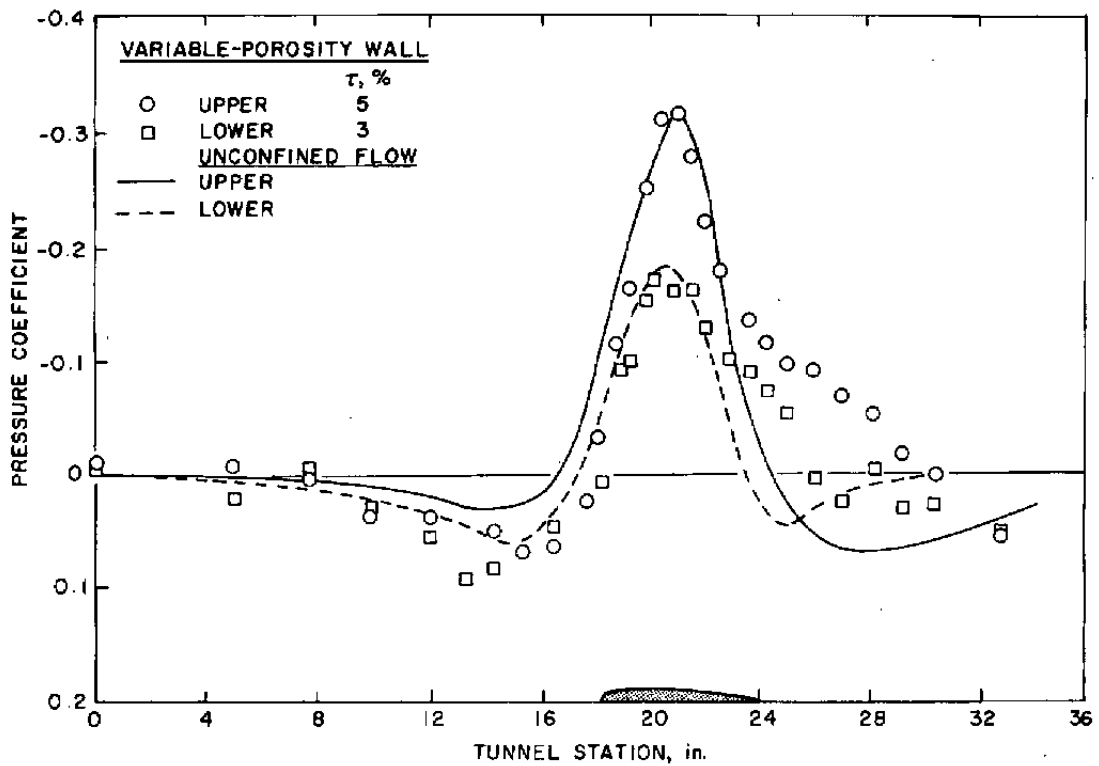
Figure 28. Control surface pressure distribution for differential top and bottom wall porosity, $M_\infty = 0.8$ and $a = 1$ deg.
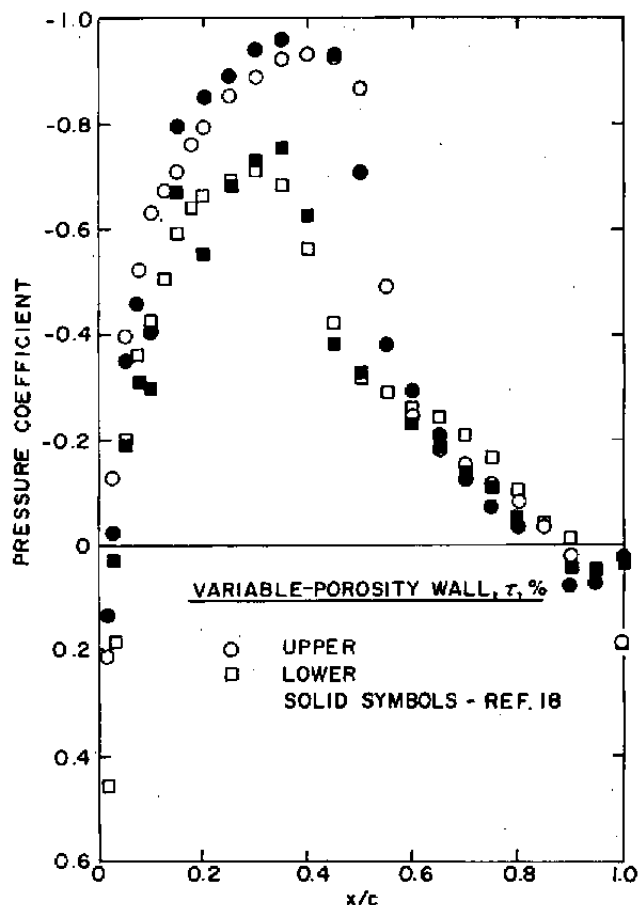
Figure 29. Model surface pressure distribution for differential top and bottom wall porosity, $M_\infty = 0.8$ and $\alpha = 1$ deg.

7.0 CONCLUDING REMARKS

Studies of the adaptive-wall concept have verified that convergence to unconfined flow has been found by application of the exterior-region computations to wind tunnel experiments. Basic two-dimensional experiments have been performed using an NACA 0012 wing model and two controllable wall configurations.

The experiments demonstrated that adaptive-wall techniques can significantly reduce wall interference effects and can eliminate large solid blockage and lift interference effects. Two parameters important to consider are the upstream static pressure level and the value of the minimum pressure, or peak, in the vicinity of the model. Adjusting the upstream pressure level to that indicated for unconfined flow from the exterior computations compensated for free-stream Mach number errors caused by the model solid blockage.

Adjusting the value of the minimum, or peak, pressure at the upper and lower control surfaces significantly reduced the lift interference effects. Both of the above results could be obtained with global wall-boundary control (consisting of uniform wall porosity and plenum pressure adjustments) although the required control surface pressure could not be matched at all tunnel stations.

The local porosity control obtained with the LVHA wall was not sufficient to effect refinement of the control surface distribution downstream of the model location. Some control over the downstream distribution was realized from adjusting the pressure ratio across the test section, but a single, uniformly applicable criterion for making this adjustment was not found.

REFERENCES

1. The Wind Tunnel Testing Techniques Subcommittee of the Fluid Dynamics Panel. "A Further Review of Current Research Related to the Design and Operation of Large Wind Tunnels." AGARD-AR-105, August 1977.

2. Binion, T. W., Jr. and Lo, C. F. "Application of Wall Corrections to Transonic Wind-Tunnel Data." AIAA Paper No. 72-1009. AIAA 7th Aerodynamic Testing Conference, Palo Alto, CA, September 13–15, 1972.

3. Binion, T. W., Jr. "An Investigation of Three-Dimensional Wall Interference in a Variable Porosity Transonic Wind Tunnel." AEDC-TR-74-76 (AD787658), October 1974.

4. Lo, Ching-Fang and Oliver, R. H. "Subsonic Lift Interference in a Wind Tunnel with Perforated Walls." *Journal of Aircraft*, Vol. 7, No. 3, May—June 1970, pp. 281-282.

5. Jacocks, J. L. "Determination of Optimum Operating Parameters for the AEDC-PWT 4-Ft. Transonic Tunnel with Variable Porosity Test Section Walls." AEDC-TR-69-164 (AD857045), August 1969.

6. Jacocks, J. L. "Evaluation of Interference Effects on a Lifting Model in the AEDC-PWT 4-Ft. Transonic Tunnel." AEDC-TR-70-72 (AD868290), April 1970.

7. Lo, Ching-Fang, "Wind-Tunnel Wall Interference Reduction by Streamwise Porosity Distributions." *AIAA Journal*, Vol. 10, No. 4, April 1972, pp. 547-550.

8. Lo, Ching-Fang and Glassman, H. N. "Calculation of Interference for a Porous Wall Wind Tunnel by the Method of Block Cyclic Reduction." AEDC-TR-75-98 (ADA017706), November 1975.

9. Kraft, E. M. "An Integral Equation Method for Boundary Interference in Perforated-Wall Wind Tunnels at Transonic Speeds." AEDC-TR-76-43 (ADA023493), April 1976.

10. Ferri, Antonio and Baronti, Paolo. "A Method for Transonic Wind Tunnel Corrections." *AIAA Journal*, Vol. 11, No. 1, January 1973, pp. 63-66.

11. Sears, W. R. "Self-Correcting Wind Tunnels." Calspan Report No. RK-5070-A-2, July 1973.

12. Erickson, J. C., Jr. and Nenni, J. P. "A Numerical Demonstration of the Establishment of Unconfined-Flow Conditions in a Self-Correcting Wind Tunnel." Calspan Report No. RK-5070-A-1, November 1973.

13. Lo, C. F. and Kraft, E. M. "Convergence of the Adaptive-Wall Wind Tunnel." *AIAA Journal*, Vol. 16, No. 1, January 1978, pp. 67-72.

14. Vidal, R. J., Erickson, J. C., Jr., and Catlin, P. A. "Experiments with a Self-Correcting Wind Tunnel." AGARD Conference Proceedings No. 174 — Wind Tunnel Design and Testing Techniques. Advisory Group for Aerospace Research and Development, Paris (France), March 1976.

15. Chevallier, Jean-Pierre. "Soufflerie Transonique a Parois Auto-Adaptables." AGARD Conference Proceedings No. 174 — Wind Tunnel Design and Testing Techniques Advisory Group for Aerospace Research and Development, Paris (France), March 1976.

16. Goodyer, M. J. "A Low Speed Self Streamlining Wind Tunnel." AGARD Conference Proceedings No. 174 — Wind Tunnel Design and Testing Techniques. Advisory Group for Aerospace Research and Development, Paris (France), March 1976.

17. Ponteziere, J. and Bernard-Guelle, R. "E'tude Experimentale des Corrections de Parois a Rich." *L'Aeronautique et l'Astronautique*, No. 32, 1971, pp. 41-52.

18. Vidal, R. J., Catlin, P. A. Chudyk, D. W. "Two-Dimensional Subsonic Experiments with an NACA 0012 Airfoil." Calspan Report No. RK-5070-A-3, December 1973.

19. Chew, W. L. "Experimental and Theoretical Studies on Three-Dimensional Wave Reflection in Transonic Test-Sections — Part III: Characteristics of Perforated Test Section Walls with Differential Resistance to Cross-Flow." AEDC-TN-55-44 (AD-84158), March 1956.

20. Parker, R. L. and Jacocks, J. L. "Evaluation of Transonic Wind Tunnel Wall-Interference Effects for Several Test Section Wall Configurations." AEDC-TR-76-125 (ADB013149L), August 1976.

21. Reed, T. D., Pope, T. C., and Cooksey, J. M. "Calibration of Transonic and Supersonic Wind Tunnels." NASA-CR-2920, November 1977.

22. Vidal, R. J. and Erickson, J. C., Jr. "Research on Adaptive Wall Wind Tunnels." AEDC-TR-78-36 (ADA062110), November 1978; Calspan Report No. RK-5934-A-1.

23. Lo, C. F. and Sickles, W. L. "A Hybrid Method of Transonic Computation with Application to the Adaptive Wind Tunnel" Presented at the Eighth U. S. National Congress of Applied Mechanics, Los Angeles, CA, June 26-28, 1978.

24. Parker, R. L. "Flow Generation Properties of Five Transonic Wind Tunnel Test Section Wall Configurations." AEDC-TR-75-73 (ADA014260), August 1975.

25. Jacocks, J. L. and Parker, R. L., Jr. "Suppression of Perforated Wall Noise in a Transonic Wind Tunnel and the Effects on Aerodynamic Data." AEDC-TR-78-20 (ADA054417), May 1978.

26. Mokry, M., Peake, D. J., and Bowker, A. J. "Wall Interference on Two-Dimensional Supercritical Airfoils Using Wall Pressure Measurements to Determine the Porosity Factors for Tunnel Floor and Ceiling." NRC (Canada) LR-575 (NRC 13894), February 1974.

NOMENCLATURE

C_p — Pressure coefficient, $(p - p_\infty)/q_\infty$

c — Chord

h — Control surface location

K — Transonic similarity parameter, $K = \beta^2/M_\infty t^{2/3}$

k — Relaxation factor

LVHA — Longitudinally variable hole angle wall

M_∞ — Free-stream Mach number

P — Static pressure, psf

P_T — Total tunnel pressure

P_c — Plenum chamber pressure, psf

p_{d_e} — Pressure at diffuser exit, psf

p_o — Stagnation pressure, psf

p_∞ — Free-stream static pressure, psf

q_∞ — Free-stream dynamic pressure, psf

S — Control surface interfacing interior/exterior region

T_o — Stagnation temperature

TPR — Test pressure ratio, p_o/p_{d_e}

t — Thickness ratio, y/c

u — Nondimensional streamwise component of disturbance velocity

u_∞	Nondimensional streamwise component of disturbance velocity given by one-step formula
v	Nondimensional normal component of disturbance velocity
X	Streamwise coordinate
x/c	Nondimensional streamwise airfoil coordinate
y	Vertical coordinate
α	Angle of attack
β	$\beta = (1 - M_\infty^2)^{1/2}$
γ	Specific heat ratio, $\gamma = 1.4$
θ	Flow angle in vertical plane relative to control surface
θ_H	Wall hole angle
ϕ	Velocity potential normalized by free-stream velocity

SUBSCRIPTS

E	Region exterior to the control surface
T	Measured value in wind tunnel

SUPERSCRIPT

~	Transonically scaled variable